

Development of Fe-doped SnO₂- based nanocomposites prepared by single-step laser pyrolysis

R. ALEXANDRESCU^{*}, I. MORJAN², F. DUMITRACHE, R. BIRJEGA, C. FLEACA, C. R. LUCULESCU, E. POPOVICI, I. SOARE, I. SANDU, E. DUTU, G. PRODAN^a

National Institute for Lasers, Plasma and Radiation Devices, P.O. Box MG 36, R-077125, Bucharest, Romania.

^aOvidius University of Constanta, Constanta, Romania

We report a new synthesis technique for the preparation of Fe-SnO₂, namely the CO₂ laser pyrolysis of gas phase reactants. Tetramethyl tin, air and iron pentacarbonyl were used as precursors. At increased oxygen in mixtures, the SnO₂ phase (mean crystallite sizes about 12 nm) largely prevails over the other two crystallographic phases: SnO and Sn. Different Fe/Sn ratios (from about 0.01 to 0.08 in at %) were obtained by varying the process parameters. No iron compounds were identified by diffraction techniques. With increased Fe doping, an overall decrease of the diffraction peaks and an inhibited particle growth may be observed.

(Received June 17, 2009; accepted October 8, 2009)

Keywords: Tin oxide, Nanoparticles, Laser pyrolysis, Fe doped SnO₂

1. Introduction

Tin oxide (SnO₂) with the rutile structure is a promising functional n-type semiconductor material with a wide band-gap ($E_g = 3.65$ eV at 300 K) with high simultaneous electrical conductivity, optical transparency in the visible region of the spectrum [1] and catalytic properties [2]. Different synthesis methods were proposed for the obtaining of tin oxide nanostructures, either in the form of thin films, nanoparticles or thick films. As examples, we could mention; flame-made, thermophoretic [3] and electrophoretic [4] deposition processes, aerosol flow reactor [5], electrochemical synthesis [6], arc plasma source [7], sol-gel method [8].

It has been suggested that the introduction of Fe^{III} sites could lead to improvement to the initial SnO₂-based sensor or catalytic systems [9] i.e. the energy gap gradually decreases by increasing the Fe doping level [10]. The developing of dilute magnetic semiconductors with room temperature ferromagnetism has been the subject of interest for a new generation of spin electronics. Tin oxide doped with Fe showed remarkable strong ferromagnetism for which novel ferromagnetic exchange mechanisms are considered (interactions between magnetic impurities, which can be mediated either by oxygen, or by free carriers, etc) [11,12].

Structural changes associated with the doping are dependent on the synthesis method. This statement is particularly true in case of bottom-up approaches (such as colloidal or aerosols methods of preparation [7]) where process control over particle surface and size dimensions was noticed. One commonly encountered problem is that these methods are generally at least two steps methods. In our previous studies we have successfully reported on the synthesis of iron oxide nanostructures using the laser

pyrolysis route as a single-step reaction route [13]. It is important to note that the IR laser pyrolysis technique is a gas phase technique, which allows for the preparation of a large variety of nano bodies with diameters ranging from a few nm to about 100 nm and with narrowly distributed sizes [14].

The in-situ synthesis of SnO₂-based nanoparticles using the pyrolysis of tetramethyl tin sensitized with ethylene mixtures is demonstrated in this work. Simultaneously, iron co-doping (at low Fe concentrations) was performed, introducing iron pentacarbonyl in the reactive mixture. Depending on the experimental parameters, different amounts of SnO₂ and SnO with traces of the metallic Sn were obtained. At a higher air concentration (the reaction oxidizing agent) major SnO₂ content was found. According to our knowledge, the synthesis of Fe doped tin oxide by using the laser pyrolysis from gas-phase precursors is reported for the first time. Much more, our study concerns low-concentration Fe-doped tin oxide nanocomposites which is a domain rarely approached in the literature. Controlled Fe/Sn atomic ratios, ranging from nominal 0 to 0.08 were used in order to prepare Fe-doped SnO₂-based nanopowders. The effects of the iron-dopant concentration on the essential structural properties of the resultant powders such as the phase formation, the crystallinity, the average particle size and distributions were systematically investigated.

2. Experimental details

The laser synthesis technique is based on the resonance between the emission of a CW CO₂ laser line and the infrared absorption band of a gas precursor. The chemical reaction is triggered by the subsequent heating of

precursors by collisional energy transfer. In this paper the synthesis of pure and Fe-doped tin oxide nanopowders was performed by employing a modified version of the pyrolysis set-up [13] in which tetramethyl tin (TMT), iron pentacarbonyl ($\text{Fe}(\text{CO})_5$) and air, as gas phase precursors are simultaneously allowed to emerge into the flow reactor (Fig.1). Ethylene served as a carrier for the TMT and $\text{Fe}(\text{CO})_5$ vapors and as an energy transfer agent. Complementary Ar flows are employed for the confinement of reactant gases/nucleated particles towards the flow axis and for flushing the windows, respectively. The focused IR radiation (100 W nominal power) was intersecting at right angles the reactant flows. The aggregation of the hot, freshly nucleated particles is rapidly stopped by the sudden cooling/ freezing outside the reaction zone.

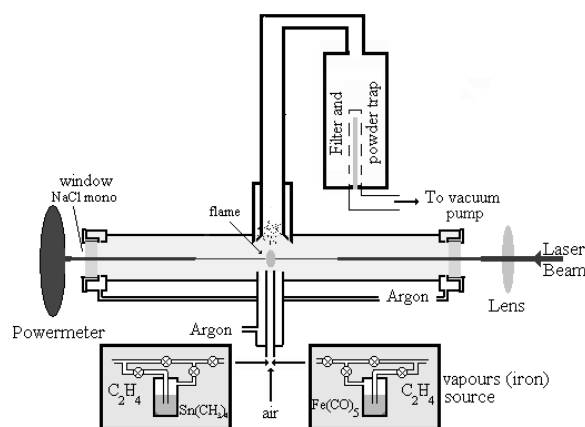


Fig. 1. Experimental setup for the preparation of Fe-doped SnO_2 -based mixtures by the sensitized laser pyrolysis.

Table 1. Experimental synthesis parameters and EDAX results for the prepared pure and doped tin oxide samples. In the experiments, the following parameters were maintained constant: the pressure (50 000 Pa (500 mbars)), the laser power (65 W), the argon confinement flow (1500 sccm) and the Ar flows for windows cleaning (150 sccm).

Sample	Φ_{air} sccm	$\Phi_{\text{C}_2\text{H}_4}$ through $\text{Sn}(\text{CH}_3)_4$ sccm	$\Phi_{\text{C}_2\text{H}_4}$ through $\text{Fe}(\text{CO})_5$ sccm	EDAX Measurements at%						
				C	O	Sn	Fe	Sn/O	C/(Sn+Fe)	Fe/Sn
SnO4	150	30	-	11.64	51.37	36.99	-	0.71	0.31	-
SnO5	200	30	-	14.48	56.03	29.49	-	0.53	0.49	-
SnOFe3	180	30	1	9.06	60.49	29.85	0.60	0.49	0.29	0.02
SnOFe2	180	30	3	12.18	55.54	31.12	1.16	0.56	0.37	0.04
SnOFe6	180	30	6	11.77	58.14	27.62	2.46	0.47	0.42	0.08

3. Results and discussions

The XRD analysis of SnO_2 -based pure and Fe-doped samples reveals the coexistence of three major phases: i) SnO_2 - cassiterite (JCPDS 41-1445); ii) SnO -romarchite (JCPDS 06-0395) and iii) metallic Sn (04-0673). The relative amounts of these phases are different, depending on the synthesis conditions. The superposed diffraction

Two sets of representative undoped and doped tin oxide powder samples are discussed in this paper. The first series concerns undoped samples (labeled SnO4 and SnO5) which are studied relatively to the input variation of their oxygen precursors. The second series refers to three representative composite SnO_2/Fe samples (labeled SnOFe2, SnOFe3, and SnOFe6) which are characterized by low carbonyl flows and increasing Fe concentration. They are analyzed according to their input Fe/Sn atomic ratio, in comparison with the reference SnO_2 -based undoped samples. The Fe/Sn ratios loaded in the laser induced reaction were adjusted by varying the $\text{Fe}(\text{CO})_5$ flow. The main experimental parameters are listed in Table 1. In the experiments, the following parameters were maintained constant: the pressure (500 mbar), the laser power (65 W), the argon flows (1500 and 150 standard cubic centimeters per minute (sccm), for the confinement and for windows cleaning, respectively). The reaction temperature, as recorded with an optical pyrometer varied between 610 and 630 °C. In the last column of Table 1, the average values (in at %) given by X-ray energy dispersive analysis (EDAX), including the Fe/Ti and Sn/O atomic ratios in powders are displayed.

The XRD patterns were collected on a PANalytical X'Pert MPD theta-theta system in continuous scan mode (counting 2s per 0.02 2 θ). In the diffracted beam a Ni filter, a curved graphite monochromator and a programmable divergence slit were used ($\lambda=0.15418$ nm). XRD data were analyzed using the PANalytical X'Pert HighScore Plus software package. Transmission electron microscopy (TEM), high resolution transmission electron microscopy (HRTEM) and Selected Area Electron Diffraction (SAED) were used to characterize the powders.

lines in Fig. 2 compares the pure sample SnO5 with the sample with the highest Fe doping degree (sample SnFeO6), both samples sharing a high oxygen content. Many sharp peaks can be clearly indexed to the tetragonal rutile structure of SnO_2 with lattice constants of $a = 0.4738$ nm and $c = 0.3187$ nm (JCPDS 41 - 1445). SnO and Sn appear as minor phases.

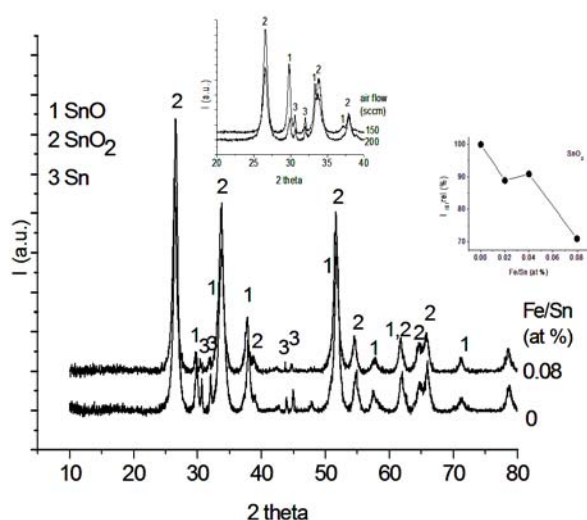


Fig. 2. XRD analysis for representative Fe-doped tin oxide (upper diffractogram of the sample SnOFe6 with the ratio (in at %) Fe/Sn = 0.08) as compared to the reference undoped sample (lower diffractogram of sample SnO5), with SnO₂, SnO and Sn peak identification. The upper inset displays the comparative XRD analysis (in the 20-48 2θ domain) for pure tin oxide samples at increasing oxidizer flows (samples SnO4 and SnO5). The lower inset presents the evolution of the (110) SnO₂ diffraction line intensity with increasing Fe concentration.

Estimations about the crystallographic phases and the Scherrer crystallite sizes are listed in Table 2. Considering

the width at half height of the most intense maxima of the two oxide phases ((101) and (110) for the SnO and SnO₂ phases, respectively) the crystallite dimensions were estimated from the Debye-Scherrer equation. In case of the Sn phase, the crystallite dimension was averaged over the two Sn intense maxima (200) and (101). For clarity, the absolute maxima of the crystallographic phases under discussion are also listed in II (columns 4, 5 and 6 for SnO₂, SnO and Sn, respectively). The next column in Table 2 presents the evolution of the SnO₂ relative intensity i.e. relatively to the ensemble of the two oxide phases. This value is deduced from the ratio between the most intense reflections of SnO₂ and the sum of the two oxide phases, i.e. $I_{110-SnO_2} / (I_{101-SnO} + I_{110-SnO_2})$. It may be clearly observed that excepting the sample obtained at a low oxidizer flow, SnO₂ is prevalent in all runs, at most in the sample doped with the highest Fe concentration (the relative intensity of the SnO₂ phase in SnOFe6 gives a value of 0.92 – see Table 2).

The XRD patterns for pure tin oxide samples at increasing oxidizer flows (samples SnO4 and SnO5) are found in the right upper insert of Fig.2. The increased air flow for sample SnO5 is leading to an inhibition of SnO and Sn phase formation simultaneously to a dominance of the SnO₂ phase: indeed, one observes an increase (of about 1.5 times) of the SnO₂ phase and a drastic decrease of the SnO and Sn phases (of about 5 times and 2 times, respectively) (see Table 2). The sample SnO4 presents higher crystallite dimensions for all three phases while for sample SnO5, lower crystallite sizes especially as regarding the dominant SnO₂ phase are revealed.

Table 2. Comparative XRD evaluation of some of the structural parameters for the pure and Fe-doped tin oxides-based mixtures*.

Sample	Fe/Sn (at %)	Intensities			Relative intensities of SnO ₂ phase $I_{110-SnO_2} / (I_{101-SnO} + I_{110-SnO_2})$	Mean Crystallite Dimensions		
		SnO ₂ I ₁₁₀	SnO I ₁₀₁	Sn I ₁₀₁ +I ₂₀₀		D-SnO ₂ (nm)	D-SnO (nm)	D-Sn (nm)
SnO4	0	1917	2135	901	0.47	14.9	23.2	46.2
SnO5	0	2161	457	439	0.83	13.1	20.1	46.2
SnOFe3	0.02	2002	390	401	0.84	11.3	25.0	41.9
SnOFe2	0.04	1973	381	452	0.83	12.0	31.1	47.0
SnOFe6	0.08	1783	165	161	0.92	13.2	38.8	49.1

* The XRD measurement conditions for all samples were strictly maintained at constant parameters, i.e. values of 33 kV and 18 mA were used for the tube power and 2 s per step was chosen as acquisition time.

It is worth to note that according to Ref. [15], rather low reaction temperatures (around 500 °C) and short heating times (specific for the high temperature gradients developing during milliseconds in the laser pyrolysis) could favor the coexistence of SnO₂, SnO and Sn phases.

It is known that SnO₂ (stannic oxide) possesses the rutile structure and SnO (stannous oxide) has the less common litharge structure. Stannic oxide is the more abundant form of tin oxide. The heats of formation for stannous and stannic oxides at 298 K were determined as $D_H = 68$ cal/mol and $D_H = 138$ cal/mol, respectively [2]. This results of $D_H = 70$ cal/mol for the reaction $\text{SnO} + 1/2 \text{O}_2 \rightarrow \text{SnO}_2$ which proves that complementary thermal energy is needed for the formation of stoichiometric SnO₂ (implying the Sn⁺⁴ valence state).

The diffractograms of Fe-doped samples (SnOFe2, SnOFe3 and SnOFe6) present many similar features to the pure sample SnO5 (illustrated in Fig. 2 for SnOFe6) namely a major SnO₂ phase and much lower amounts of SnO and Sn phases. This resemblance could be due to a combination of causes between which i) the rather similar oxidizing conditions (in the case of Fe-doped samples the air flow of 200 sccm was very near the 180 sccm air flow of Fe-doped samples), ii) the role played by iron during the induced reaction and iii) the very low doping degree of samples.

It is worth to underline that no Fe compounds could be detected by X-ray analysis. It seems however that the presence of Fe favors oxidation. There are several reports in the literature confirming that even at higher Fe concentration XRD does not clearly reveal the presence of iron compounds [12,16]. This fact is attributed to a temperature effect (occurring below 650 °C) and demonstrates that Fe atoms are soluble in SnO₂ crystallites [16].

A main effect observed by XRD with increasing iron concentration is an overall decrease of diffraction line intensities for all the three SnO₂/SnO/Sn phases. This statement may be observed from the evolution of the absolute intensities of the most intense maxima (see Table II) and is illustrated for the SnO₂ [110] line intensity in Fig.2 - the right, lower inset. Due to the fact that all samples were recorded in strictly the same conditions (see the Experimental section) this intensity decay could be explained as well by the perturbation induced by iron in the crystallographic structure as by increased X-ray absorption of Fe-containing samples.

The evolution of the mean crystallite dimensions with increasing Fe-doping level (the last columns in Table II) seems to present different tendencies relatively to the chemical components of the nanocomposite. We should stress first the low crystallite dimensions exhibited by the dominant SnO₂ phase relatively to the SnO and Sn phases. With increasing Fe content, the crystallite size remains almost unaffected (about 12 nm) for SnO₂, even if a very slight decrease is observed at the first doping step. The crystallite dimensions of the minor Sn phase follow the same trend (the mean crystallite size is about 45 nm). In the case of SnO the crystallite size seems to slightly increase with iron concentration (from about 20 nm to

58 nm). It is worth to mention that different authors [11, 12,16,17] have reported that the doping of Fe can prevent the growing-up of SnO₂ crystallites. Much more, for higher temperatures (above 650 °C [16]) and higher Fe concentrations (about 3 at% Fe [17]) a decreased trend of SnO₂ crystallite dimensions was observed. The inhibition role of Fe regarding the formation of SnO₂ phases was attributed in Ref. [11] to a substitutional replacement of Sn⁴⁺ ions by transition metal ions of lower charge (Fe³⁺). Because of the smaller size of most of the transition metal ions compared to Sn⁴⁺ ions, a lattice contraction is expected. Thus, under compressive strain the grain size of the nanoparticles decreases [17].

Summarizing, XRD analysis reveals that the sample containing the highest SnO₂ percent relatively to SnO and Sn phases is SnOFe6 (characterized by the highest Fe concentration). The crystallite dimensions of the dominant SnO₂ phase are very low as compared to the other components and kept almost constant in the frame of the present experimental conditions.

The EDAX measurements (in at%) of pure and Fe-doped samples (the last columns in Table I) point to the increasing Fe/Sn ratio, according to the increased supply in the Fe(CO)₅ vapor precursor. Excepting sample SnO4 (with Sn/O=0.7) for which the deficient oxygen favors higher amounts of SnO and Sn (as observed in XRD analysis), EDAX reveals that Sn/O ratios near 0.5 (values ranging from 0.49 to 0.56) are obtained for all samples. This fact could indicate that for the samples mentioned above the stoichiometric tin oxide could prevail, in accordance with the XRD findings. Carbon contamination is found in samples due to the unwanted ethylene sensitizer decomposition. It is the only absorber of the IR laser radiation and at the same time it is the carrier for Fe(CO)₅ and TMT vapors. Either an increased oxygen supply (sample SnO5) or a higher C₂H₄ amount in the reaction zone (sample SnOFe6) may lead to an increasing reaction temperature which in turn speeds up the C₂H₄ decomposition. Indeed, as shown in Table I, the ratio C/(Sn + Fe) in at% increases from 0.31 to 0.49 (at increased oxidizer flow) and from 0.29 to 0.42 in case of the Fe-doped samples (for increased ethylene carrier of the Fe(CO)₅ vapors).

Low-magnification TEM micrographs for undoped and Fe doped SnO₂-based samples show groups of loosely-bound aggregated nanoparticles. Fig. 3 displays the TEM image (magnification 87000 x) of sample SnO5. The respective grain size histogram is given as inset. It reveals a bimodal distribution (lognormal fitted). It is probable that this distribution accounts for the large difference between the mean diameters of the two main groups, the first one comprising the prevalent stoichiometric tin oxide (SnO₂) with about 13 nm mean particle diameter and the second one including the Sn and/or SnO minor components with about 38 nm mean diameter.

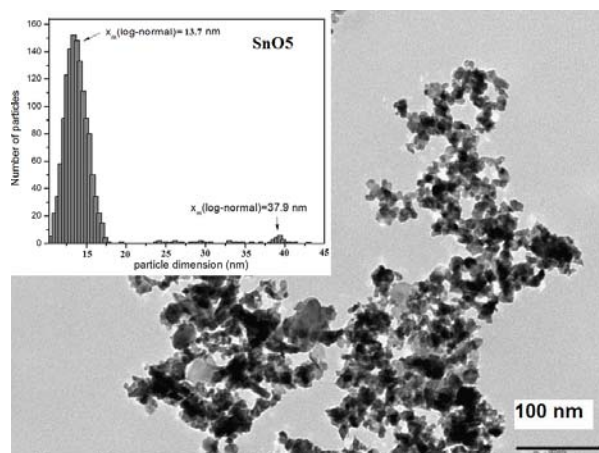


Fig. 3. Typical TEM view (magnification 87000 \times) of the undoped sample SnO₅ (obtained at a high oxidizing flow). Its respective grain size histogram (lognormal fitted) is given as inset (see text).

It may be observed that in the TEM image it is hard to discriminate between Sn and SnO nanoparticles. The restrained growth upon iron doping with increasing Fe/Sn ratio (from 0 to 0.08) further keeps the mean particle sizes in the same range of their respective values. Consequently, the TEM images with the same magnification for Fe-doped samples present similar features and particle distributions, suggesting a low concentration of the minor Sn and SnO particles (in agreement with XRD findings).

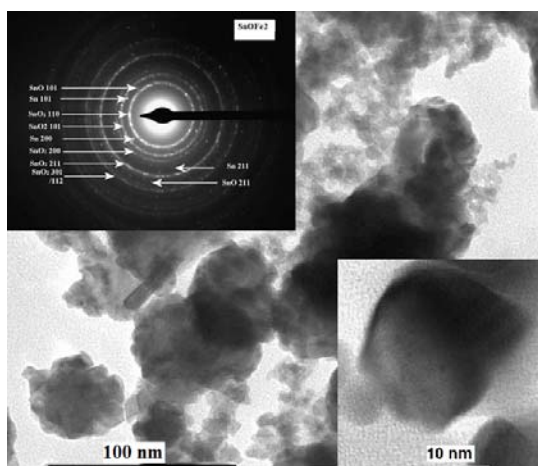


Fig. 4. TEM micrograph of a Fe-doped sample (SnOFe₂) at a higher magnification (145000 \times) and the corresponding SAED pattern (upper, left inset). HRTEM images of a primary faceted nanocrystal at 1050000 \times magnification (right, lower inset).

However, due to the appearance of new morphological details we present further the TEM micrograph of a Fe-doped sample (SnOFe₂) at a higher magnification (145000 \times) (Fig. 4). Large dark balls (about

30–40 nm diameter) which could belong to Sn metal are encased with much smaller, aggregated particles (about 10 – 15 nm mean size). These more numerous small particles (probably SnO₂) have a fluffy appearance and are spreading all over the picture. The segregation of some kind of core-shell structures was observed in Ref. [15]. It was attributed to a kinetically controlled mechanism where the fast oxidation of tin did not proceed to completion and sequential, core-shell structures could form and stabilize over the entire material.

At a higher magnification (1050000 \times) the HRTEM image of a primary faceted nanocrystal (about 14 nm diameter) is presented (right inset in Fig. 4). The particle shows irregular, quasi-prismatic shape, possibly surrounded by an amorphous layer.

The associated SAED pattern for the particles of sample SnOFe₂ (Fig. 4) is presented in the left inset of this Figure. The identification of the interplanar distances is indicated by arrows. The indexing of the diffraction rings evidences the three Sn-based phases which reveal the main diffraction rings for SnO₂ (3.35, 2.64, 2.36, 1.76, 1.41, 1.44 Å), for SnO (2.99, 1.60 Å) and for Sn (2.90, 2.78, 2.02 Å). The most intense diffraction ring can be assigned to cassiterite SnO₂ and appears at 0.335 nm. No direct evidence of Fe incorporation was found. A direct comparison of the SAED values with the results obtained by means of XRD demonstrates a good agreement between these two analytical methods. On the other hand, it has been recognized that XRD and SAED are not sensitive enough to identify small amounts of impurity phases (such as Fe or Fe compounds) in the samples.

4. Conclusions

Undoped and iron doped SnO₂-based nanoparticles with low Fe concentration have been successfully synthesized by using the IR laser pyrolysis from gas phase reactants. (CH₃)₄Sn and Fe(CO)₅ in ethylene sensitized mixtures were employed as vapor-phase precursors. As concerning the Fe-doped SnO₂ nanopowders, controlled Fe/Sn atomic ratios (in at %) ranging from nominal 0 to 0.08 were achieved in a one-step pyrolysis process. From the three identified crystalline phases (SnO₂, SnO and Sn,) the clear dominance of the SnO₂ phase at higher oxygen precursor flow was found. No iron compounds were detected. According to XRD, the major effects of iron doping are: i) an overall decrease of the diffraction peaks of the three phases with increased Fe doping (which could be explained by the perturbation induced by iron in the crystallographic network); ii) an inhibited particle growth probably due to the substitutional introduction of Fe atoms. As confirmed by XRD and TEM, the mean particle dimensions of the dominant SnO₂ phase are very low (about 12 nm) as compared to the other two components and kept almost constant in the frame of the present experimental conditions.

Acknowledgements

Support of this research by the by the Project IDEI – NACOSOF-No 431/2007 of the Research Program PNCDI II of the Romanian Ministry of Education is gratefully acknowledged.

References

- [1] H. L. Hartnagel, A. L. Dawar, A. K. Jain, C. J. Jagadish, Semi-conducting transparent thin films, IOP, Bristol, 1995.
- [2] M. Batzill, U. Diebold, Progress in Surface Science, **79**, 47 (2005).
- [3] L. Mädler, A. Roessler, S.E. Pratsinis, T. Sahn, A. Gurlo, A. Barsan, U. Weimar, Sensors Actuators B **114**, 283 (2006).
- [4] M. K. Kennedy, F. E. Kruis, H. Fissan, H. Nienhaus, A. Lorke, T. H. Metzger, Sensors Actuators B, **108**, 62 (2005).
- [5] M. Adachi, K. Okuyama, Y. Kousaka, H. Tanaka, J. Aerosol Sci., **19**, 253 (1988).
- [6] W. Chen, D. Ghosh, S. Chen, J. Mater. Sci. **43**, 5291 (2008).
- [7] G. Lu, K.L. Huebner, L. E. Ocola, M. Gajdardziska-Josifovska and J. Chen, Journal of Nanomaterials vol. 2006, Article ID 60828, 7 pages, 2007. DOI: 10.1155/JNM/2006/60828.
- [8] F. Gu, S. F. Wang, M. K. Lu, G. J. Zhou, D. Xu, and D. R. Yuan, J. Phys. Chem. B, **108**, 8119 (2004).
- [9] P. G. Harrison, Chemistry of Tin, Chapman and Hall, New York, 1989.
- [10] M. Rumyantseva, V. Kovalenko, A. Gaskov, E. Makshina, V. Yuschenko, I. Ivanova, A. Ponzoni, G. Faglia, E. Comini, Sensors and Actuators B, **118**, 208 (2006).
- [11] C. Van Komen, A. Thurber, K. M. Reddy, J. Hays, A. Punnoosea J. Appl. Phys. **103**, 07D141 (2008).
- [12] J. Sakuma, K. Nomura and C. Barrero, M., Thin Solid Films **515**, 8653 (2007).
- [13] R. Alexandrescu, F. Dumitrache, I. Morjan, I. Sandu, M. Savoiu, I Voicu, C. Fleaca, R. Piticescu, Nanotechnology **15**, 537 (2004).
- [14] R. Alexandrescu, I. Morjan, I. Voicu, D. Dumitrache, L. Albu, I. Soare, G. Prodan, Appl. Surf. Sci. **248**, 138 (2005).
- [15] A. Kolmakov, Y. Zhang, and M. Moskovits, Nano Letters **3**, 1125 (2003).
- [16] W. Junbo, Y. Ming, L. Yingmin, C. Licheng, Z. Yan, D. Bingjun, Journal of Non-Crystalline Solids **351**, 228 (2005).
- [17] X. Mathew, J. P. Enriquez, C. Mejía-García, G. Contreras-Puente, M. A. Cortes-Jacome, J. A. Toledo Antonio, J. Hays and A. Punnoose, J. Appl. Phys. **100**, 073907 (2006).

*Corresponding author: rodica.alexandrescu@inflpr.ro
ralealexandrescu2001@yahoo.co.uk